A global view of the atmospheric lunar semidiurnal tide

A. R. Paulino,[1] P. P. Batista,[1] and I. S. Batista[1]

Received 12 March 2013; revised 23 October 2013; accepted 22 November 2013; published 12 December 2013.

[1] Atmospheric lunar semidiurnal tides are studied using 10 years of temperature data collected by the Thermosphere Ionosphere Mesosphere Energetics and Dynamics/Sounding of the Atmosphere Using Broadband Emission Radiometry satellite. The amplitudes and phases in the temperature field are calculated by performing least mean square fit in a data set of about 60 day interval (combining ascending and descending data together). The mean tidal structures are studied for the height range from 20 to 120 km, between ±50° latitude and centered on each month from February 2002 to January 2012. A clear signature of the 12.42 h (lunar semidiurnal tide) is observed in the data. Characteristic of propagating waves is observed in the vertical amplitude and phase profiles in almost all heights. The best conditions of propagation for the lunar semidiurnal tide are reached in the lower thermosphere region. Asymmetry between the hemispheres and seasonal variability is observed in the amplitudes of the tide. Longitudinal variations are also observed, which reveals the existence of nonmigrating components in addition to the dominant migrating lunar tide.

Citation: Paulino, A. R., P. P. Batista, and I. S. Batista (2013), A global view of the atmospheric lunar semidiurnal tide, *J. Geophys. Res. Atmos.*, *118*, 13,128–13,139, doi:10.1002/2013JD019818.

1. Introduction

[2] The existence of the atmospheric lunar tide or atmospheric gravitational tide has been recognized by Newton and was studied by Laplace, both theoretically and from barometric observations. However, for many years the attempt to identify the gravitational tide in the atmosphere failed because the available observations which were made only daily were insufficient. The first result with reliable identification was published in 1847 by Sabine using tropical pressure data at St. Helena Observatory. However, the valid determination of atmospheric lunar tide outside the tropics was obtained from the Greenwich hourly data by Chapman in 1918. Detailed information about early works on atmospheric lunar tide is given in *Chapman and Lindzen* [1970].

[3] The lunar tide is generated in the lower, denser atmospheric region primarily by the gravitational forcing of the Moon. Moreover, the vertical motions of the oceans in the lower atmosphere contribute to the generation of this tide. The lunar tide is considerably modified by the atmospheric conditions as it propagates. It is composed by different modes, but the migrating lunar semidiurnal tide (12.420 solar hour or 1.9323 cycles per day) is the most important, because it reaches the largest amplitudes.

[4] The lunar semidiurnal tide propagates vertically, achieving large amplitudes in the mesosphere and lower thermosphere (MLT). In this region, radar measurements have contributed to the understanding of the structure and characteristics of this oscillation. An interesting result that came out from radar data was the large variability of the lunar semidiurnal tide. Since this tide is excited by a predictable and well-known source, the observed variability must represent responses to the changes in the background atmosphere acting upon it. Thus, the determination of the lunar tide in the MLT is an excellent tool to understand the coupling mechanism between the lower and upper atmosphere.

[5] Recent works have shown a significantly enhanced effect of the lunar semidiurnal tide during sudden stratospheric warming in the equatorial electrojet and vertical drift velocity [*Fejer et al*., 2010; *Park et al*., 2012]. Enhanced amplitudes of the lunar semidiurnal tide in MLT winds in three Brazilian sites during the 2006 sudden stratospheric warming (SSW) were observed by *Paulino et al*. [2012]. *Pedatella et al*. [2012a] using model simulation showed that enhanced lunar tides during SSWs are of significant importance for generating the low-latitude ionosphere perturbations during these periods.

[6] Some characteristics of the lunar semidiurnal tide in the atmosphere have also been assessed by models [*Forbes*, 1982; *Vial and Forbes*, 1994; *Stening et al*., 1997]. Using simulations, *Vial and Forbes* [1994] showed the existence of seasonal behavior for the lunar semidiurnal tide in the MLT region and also predicted a latitudinal variation along the year. The importance of the background atmospheric winds and temperatures on the propagation of the lunar tide into the MLT was studied by *Stening et al*. [1997]. Additionally, the vertical characteristics of the lunar tide, from the surface to 400 km, in winds and temperature fields, have also been studied [*Forbes*, 1982].

[7] Few studies have shown the global structure of the lunar tide, for example, using GPS total electron content (TEC)

[1]Instituto Nacional de Pesquisas Espaciais, São José dos Campos, Brazil.

Corresponding author: A. R. Paulino, Instituto Nacional de Pesquisas Espaciais, Av. dos Astronautas, 1.758, São José dos Campos, São Paulo, 12227010, Brazil. (anaroberta@dae.inpe.br)

2169-897X/13/10.1002/2013JD019818

observations [*Pedatella and Forbes*, 2010] and based on magnetic field measurements by the CHAMP (Challenging Minisatellite Payload) satellite [*Lühr et al*., 2012]. The continuous temperatures measurements by the SABER (Sounding of the Atmosphere Using Broadband Emission Radiometry) instrument on the TIMED (Thermosphere Ionosphere Mesosphere Energetics and Dynamics) spacecraft make possible to study various aspects of lunar tide in a global scale. For example, *Forbes et al*. [2013] used TIMED/SABER data in order to compare the observations with the GSWM (global scale wave model) results for the lunar tide. Besides the vertical profile from 20 to 120 km for different latitudes, the present work will show the longitudinal, latitudinal, and seasonal behavior of this oscillation using temperature measured by the SABER instrument.

2. Methodology

[8] The data used in this study is the temperature measured by the SABER, which is an instrument onboard the TIMED satellite launched in December 2001, which began making observations in January 2002. The temperature profiles are retrieved from CO_2 emissions using local thermodynamic equilibrium (LTE) in the stratosphere and nonlocal thermodynamic equilibrium (non-LTE) in the MLT (for more details, see *Mertens et al*. [2001]). The SABER views the atmosphere 90° to the satellite velocity vector in a 625 km and 73° inclination orbit so that latitude coverage on a given day extends from about 53° in one hemisphere to 83° in the other. This viewing geometry alternates once every 60 days due to 180° yaw maneuvers required for the TIMED satellite. The TIMED orbit precesses to cover 24 h of local time in each 60 day yaw period, using ascending and descending data together. The retrieval errors, in addition to those associated with instrumental noise, are estimated by *Mertens et al*. [2001], and they have been found to vary from 1.4 K at 80 km and 22.5 K at 110 km. Above 110 km the results should be viewed with due caution because of uncertainties in the measurements. A detailed description of the error for retrieval temperature in LTE and non-LTE from 20 to 100 km for SABER measurements taken during typical and extreme conditions and different seasons can be found in *García-Comas et al*. [2008], *Remsberg et al*. [2008], and *Mertens et al*. [2009].

[9] The lunar signal is often small when compared to the solar tide and may also be subject of fluctuations in amplitude and phase over periods of a few days. Moreover, the solar semidiurnal tide (12 h) and lunar semidiurnal tide (12.42 h) have very close periods when they are observed by ground-based stations on the Earth. Thus, if the solar semidiurnal tide includes transient effects, its spectrum will become broadened so that energy will spread into the lunar tidal period. The shorter the data set analyzed, the greater may be the influence of this. In this way, extended data set are required to provide the necessary spectral resolution to separate the lunar and solar tides.

[10] However, from the perspective of a satellite view the wave periods of lunar and solar tides can be widely different, so the common aliasing problem between these oscillations can be avoided to a significant degree. For example, from either the ascending or descending leg of the TIMED satellite orbit, the semidiurnal lunar period is 11.86 days and the semidiurnal solar period is 60 days. The reader is referred to *Forbes et al*. [2013] and *Ray and Luthcke* [2006] for detailed discussion.

[11] We use temperature data from February 2002 to January 2012, in order to study monthly mean amplitudes and phases response of the lunar semidiurnal tide in the temperature field (hereafter, we will refer only as amplitude and phases). The lunar tide is obtained by performing the least squares fit of the form

$$\sum_{n=1}^{3} A_n \cos(n\tau + \phi_n)$$

where τ denotes lunar local time, n represents sub harmonics of a lunar day, and A_n and ϕ_n are the amplitude and phase, respectively. Solar and lunar local times are related as $\tau = t - v$ (t denotes the solar local time, and v is the age of the Moon, a cyclic term which is dependent on the phase of the Moon and where $v = 0$ is equivalent to new moon). This analysis is performed over a composite lunar day.

[12] In this analysis, a window size of ~60 days (combining ascending and descending data together) is used to obtain monthly amplitudes and phases, in order to ensure about 5 cycles of lunar semidiurnal tide. Furthermore, a grid size of ±20° in longitude and ±5° in latitude was used for obtaining at least 3 or 4 orbits per day. The background variation represented by the temperature averaged within each latitude × longitude grid is removed before the proceeding to the determination of the lunar tide.

[13] After that, each monthly value will be vector averaged for 10 years of data. Moreover, the solar tide would have no phase relationship with the position of the Moon (unlike lunar tide which by definition is well correlated). Thus, if the analyses are in lunar time, over the course of several days, the random phasing of any wave with respect to the position of the Moon will lead to self-cancelation and so such a wave should not produce a significant signal in the analyses.

[14] Figure 1 shows a composite lunar day analysis for the temperature measured by TIMED/SABER from 15 December 2002 to 15 February 2003 at 102 km altitude, centered at 30°S and 50°W. The solid line represents the least mean square fit for this data set. The composite day analysis reveals a clear lunar semidiurnal tide, which has exactly two cycles per lunar day and the amplitude reaches values as large as 10 K. This analysis indicates clear evidence that a significant lunar tide is present and can be identified in the data.

[15] In this work, monthly means of amplitude and phase are calculated for lunar tide in all months available for the period described above. The monthly means of amplitude and phase of the lunar tide for each month of successive years are then vector averaged.

3. Results

[16] Figure 2 represents the zonal average for lunar semidiurnal tide calculated over all period (2002–2012) at the latitudes 0°, 20°S, 20°N, 40°S, and 40°N for the amplitude (Figure 2, left) and phase (Figure 2, right). The mean amplitudes (Figure 2, left) grow with height from 20 km to ~110 km, where there is a peak; above the peak the amplitude decreases quickly. In general, the phase profile shows a downward phase progression. A phase

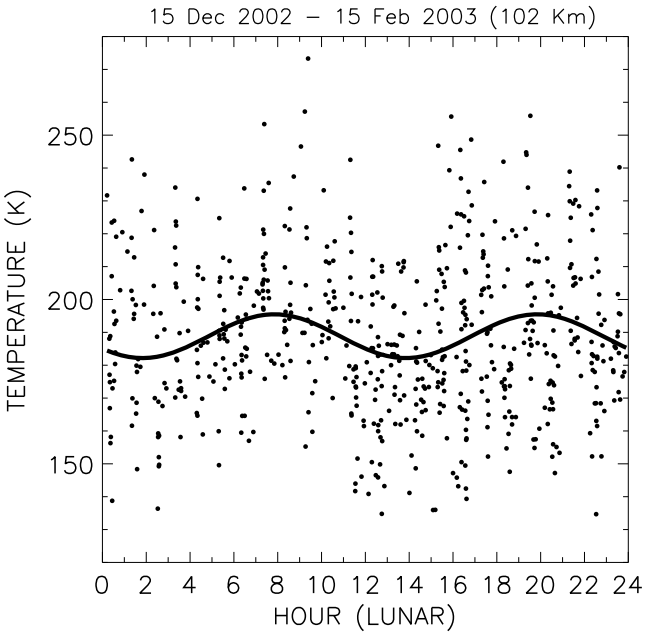

Figure 1. Composite lunar day of temperature data measured by SABER/TIMED from 15 December 2002 to 15 February 2003 at 102 km of altitude, 30°S and 50°W. The solid line represents a fit for lunar semidiurnal tide.

discontinuity is observed at ~100 km for 40°S and at ~90 km for 40°N. At 20°N between about 85 and 100 km the phase progression is in the opposite direction indicating reflection or mode coupling.

[17] Error bars in Figure 2 represent the uncertainties in the calculation plus the variability from year to year for the lunar semidiurnal tide. SABER error of the temperature field combined with the standard deviation from the least square fit is used to estimate the uncertainties in the determination of the amplitudes and phases. SABER error is performed as an input for the lunar semidiurnal tide calculation according to the results by *Remsberg et al*. [2008]. Furthermore, the uncertainties for the determination of the lunar tide follow the methodology described by *Bevington* [1969].

[18] Table 1 shows the interval of uncertainties in the determination of the amplitudes and phases for some specific heights. These intervals represent the minimum and maximum values of the uncertainties for each height. Larger values of uncertainties are obtained for high latitudes due to the reduction of available data points. Note that the error bars are due mainly to the well-known year-to-year variability [*Stening and Jacobi*, 2001; *Stening et al*., 1994], mainly in the mesosphere and lower thermosphere. Table 1 shows that the highest values of uncertainties of the amplitudes and phases appear at the lower and the upper atmosphere.

[19] Figure 3 illustrates the zonal mean amplitudes that represent the seasonal and latitudinal variability of the lunar semidiurnal tide. From November to January, the amplitudes present two peaks occurring at around ±20° latitude, with the southern peak being slightly larger than the northern peak. From February to April, the amplitudes present a single peak centered at the equator, but in February and March the values are slightly larger in the Southern Hemisphere and reverted to the Northern Hemisphere in April. In May, the peak in amplitude is observed centered in ~20°N. From June to September two peaks were again present with larger values in the Northern Hemisphere. In October, a single peak in amplitude in Northern Hemisphere is observed. The largest amplitudes are observed in December and January at around 110 km with values as large as 8 K. In general, the maximum amplitudes are observed in the solstice months. However, the values are larger in the December solstice than in the June solstice. The minimum values of amplitudes are obtained in the equinox months,

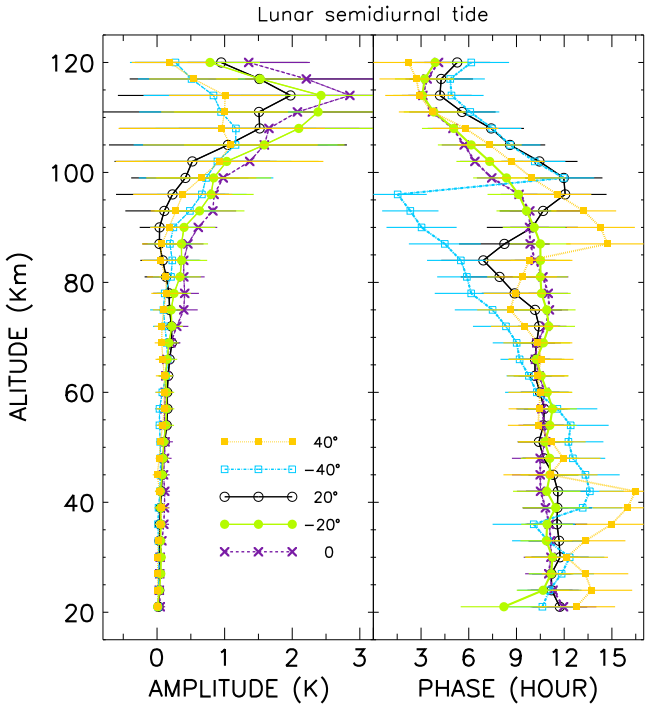

Figure 2. Vertical mean profile for lunar semidiurnal tide at 0°, 20°S, 20°N, 40°S, and 40°N latitude.

Table 1. Uncertainties for the Lunar Semidiurnal Tide

	Uncertainties (σ)	
Altitude (km)	Amplitude (K)	Phase (h)
20	0.01–1.0	0.01–2.5
40	0.01–0.5	0.09–2.0
60	0.01–0.2	0.09–1.5
80	0.01–0.3	0.09–1.0
100	0.01–1.5	0.03–2.0
120	0.01–2.0	0.05–2.2

but the amplitudes of the temperature variation are stronger during September than March. The amplitudes reach 5 K in June solstice, 8 K in December solstice, and 3 K in equinox months. The present analysis shows a clear seasonal variation in the atmospheric lunar semidiurnal tide amplitudes.

[20] Figure 4 shows the longitude and latitude variability of the lunar semidiurnal tide amplitude for March, June, September, and December at 108 km where a clear seasonal variability can be identified. In March, the amplitude is larger in Southern Hemisphere with an amplitude peak (~7 K) over South America. In June and September, the amplitudes are larger in the Northern Hemisphere. However, in December, the amplitudes are larger in the Southern Hemisphere again. September presents about four distinct peaks in longitude in the Northern Hemisphere at around ~160–135°W, ~90–40°W, ~30–50°E, and ~130–160°E. December shows similar pattern for both hemispheres. In the Northern Hemisphere, peaks are observed at ~180–160°W, ~130–90°W, 30 W to 30°E, and ~100–140°E. In the Southern Hemisphere, they are detected at around 180–160°W, 130–90°W, 45°W to 45°E, and 90–140°E.

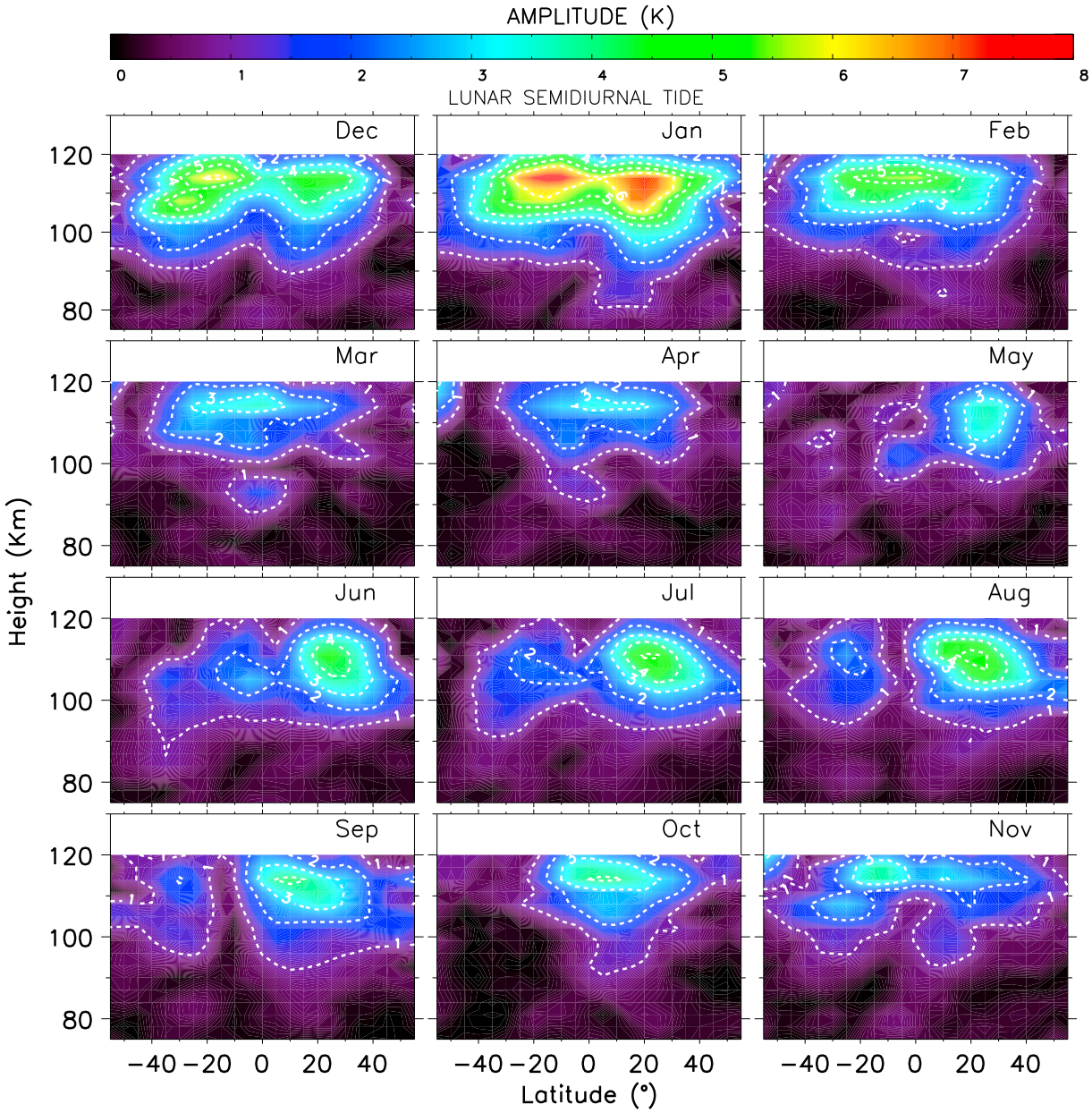

Figure 3. Average amplitude of the lunar semidiurnal tide as a function of altitude and latitude.

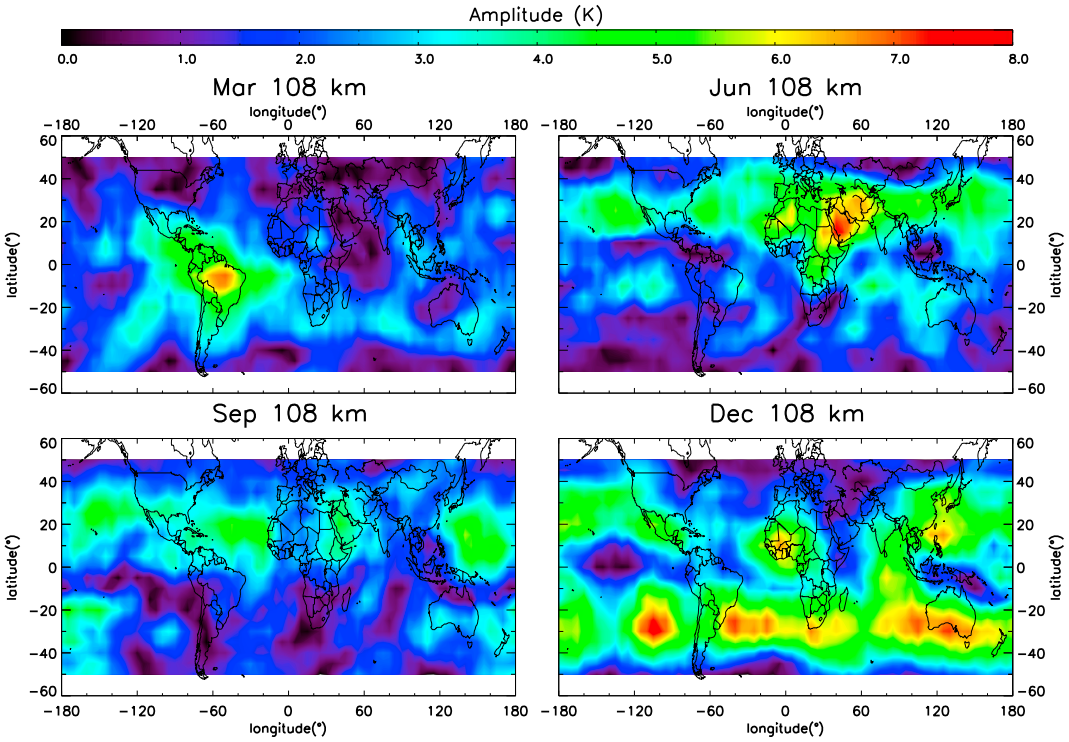

Figure 4. Monthly average latitude and longitude variability of the lunar semidiurnal tide amplitude in the temperature for March, June, September, and December at 108 km.

[21] Figure 5 provides the same information as Figure 4 and for the same period, except at 90 km. At this altitude, the lunar semidiurnal tide amplitude also presents a seasonal variability. In March, the amplitudes are larger around ± 10° latitude, with maximum values between ~ 90°W and ~ 90°E. Further, amplitudes with values between 0.9 and 1.6 are observed in the Southern Hemisphere at middle latitudes at around 160°W, 120–90°W, 45°E, and 160°E. In the Northern Hemisphere, those values are obtained at middle latitudes at about 160°W, 45–0°W, 45–90°E, and 160°E.

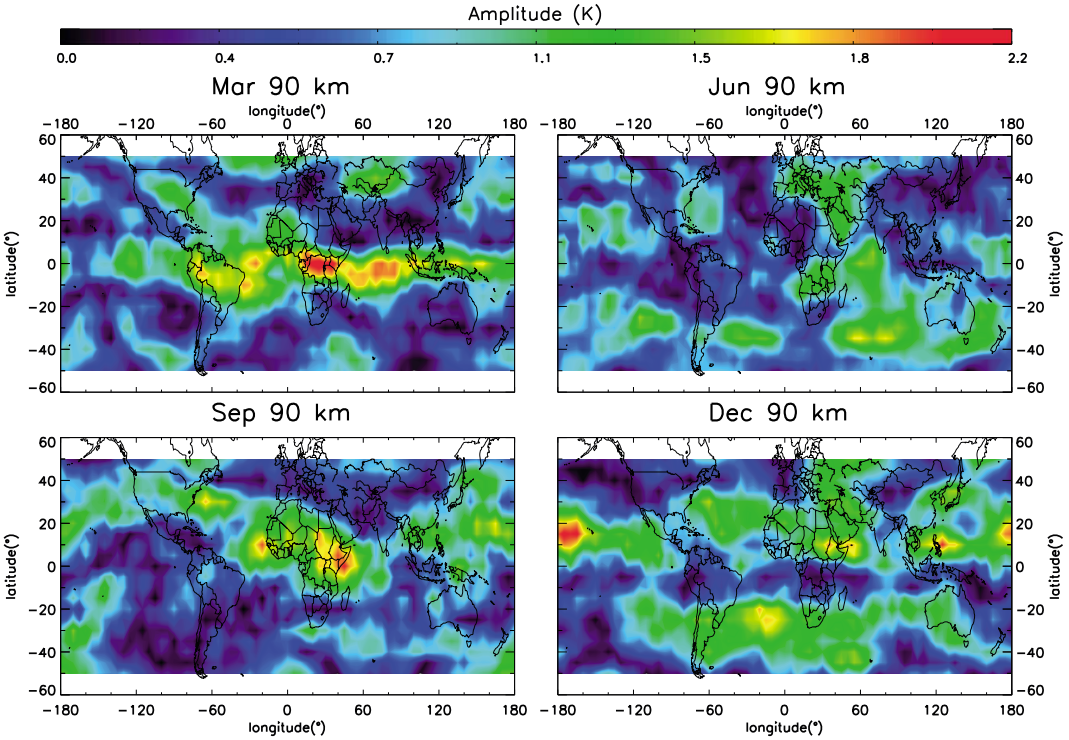

Figure 5. Same as Figure 4, except for 90 km altitude.

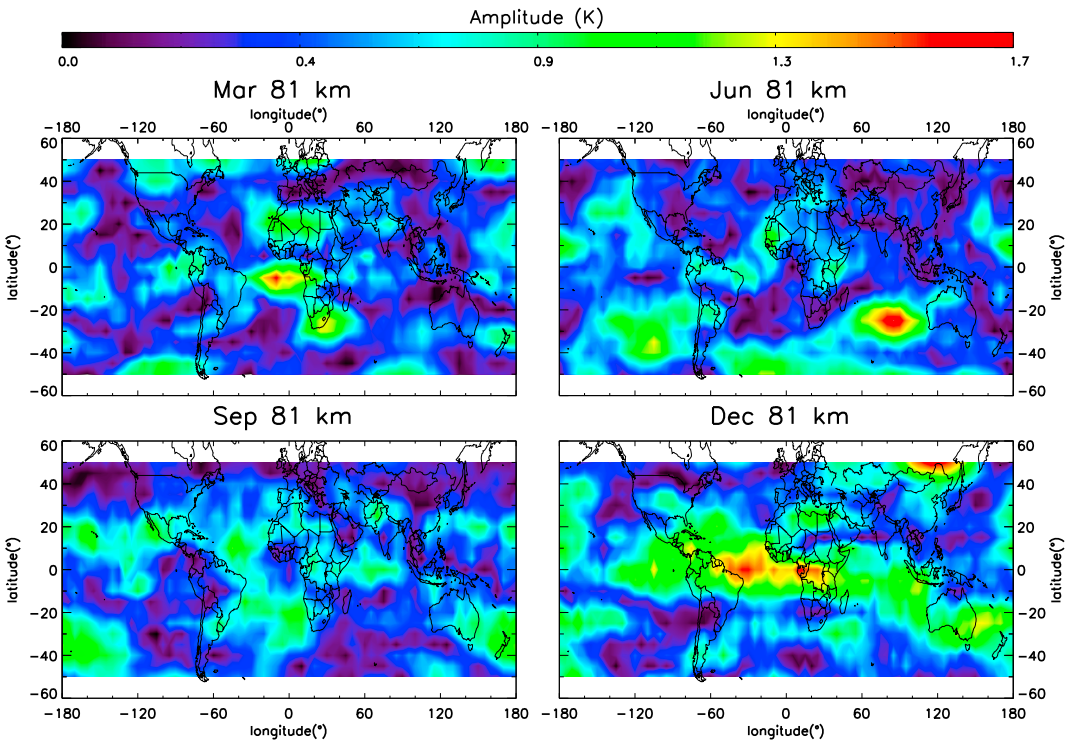

Figure 6. Same as Figure 4, except for 81 km altitude.

In June the amplitudes are larger in the Southern Hemisphere at 135–90°W, 45–0°W, 45–90°E, and 150–180°E and in the Northern Hemisphere at ~140–110°W, 90–45°W, and 0–45°E. In September, the amplitudes are larger in the Northern Hemisphere than in the Southern Hemisphere. Peaks of amplitudes are observed at 180–135°W, 90–45°W, 30°W to 45°E, and 135–180°E. In the Southern Hemisphere the amplitudes are smaller than 0.8 K in almost all longitudes. In December, the amplitudes in the Northern Hemisphere shows four peaks at 180–160°W, 60–30°W, 10–50°E, and 110–130°E. However, in the Southern Hemisphere this structure is not clear.

[22] Figure 6 is the same as Figure 4, but for 81 km. The amplitudes in March are smaller than 0.8 K in almost all longitudes in both hemispheres, except between ~30°W and 45°E. In June, the amplitudes are smaller than 0.8 K in almost all longitudes, except around 30° in the Southern Hemisphere where values higher than 1 K were observed at 135–90°W and ~60–100°E. Furthermore, at 50°S, there is one broad region of elevated amplitudes between 45°W and 130°E. In September, amplitudes are smaller than 1 K in almost all longitudes. In December a broad equatorial maximum spanning from ~135°W to ~60°E is observed.

4. Discussions

[23] As the lunar semidiurnal tide is generated at the lower atmosphere and propagates upward, one can expect that its amplitude increases with the height to conserve the energy. This pattern is clear in Figure 2 for all the latitudes studied here. When the lunar semidiurnal tide reaches the mesospheric altitudes, its development becomes faster until the maximum in amplitude, at around ~110 km height, is attained. Above that height the amplitudes show a rapid decrease. The reason for this behavior is a competition between the conditions of propagation and the dissipative processes, which become important in the thermosphere.

[24] In a theoretical work, *Forbes and Gillette* [1982] reported maximum amplitude of ~5.8 K for the lunar semidiurnal tide at around 115 km, decreasing to a minimum of 1.6 K near 160 km and then reaching very slowly varying values above 200 km at around 2 K. *Forbes* [1982] presented a study for the vertical profile of the lunar semidiurnal tide from the surface to 400 km. In that case, the amplitudes, calculated for some latitudes of the Northern Hemisphere, also increase with height, primarily, in the stratosphere, mesosphere, and lower thermosphere. The predicted maximum values for the amplitude was lower than 10 K at around 120 km height and became almost constant above this height.

[25] The mean amplitude values displayed in Figure 2 are smaller than those reported in previous works because the present analysis uses the entire 10 years data set which is vector averaged to yield mean values. This process can lead to some degree of self-cancelation of the seasonal fluctuations and/or interannual variability in the phase eventually present in the data (which is shown by the error bars in Figure 2), in such a way that the wave amplitudes become much lower than if calculated for a single month.

[26] It is noticeable that when the amplitudes increase quickly (lower thermosphere region) the phase progression with height is more pronounced. This regular progress of phase provides further confidence that a clear tidal signature has been identified. At −40° latitude, between 60 and 100 km, the vertical phase progression with height indicate vertical wavelength shorter than for the other latitudes. From 20 to 60 km where the amplitudes are small, the phase profile is almost constant with height, which means a long vertical wavelength, except at −40° and 40° latitude.

[27] As the forcing of the lunar semidiurnal tide is symmetric and the main Hough mode is the (2, 2) mode that is also symmetric, a symmetric behavior of this tide in the MLT is to be expected. However, Figure 3 reveals that for almost all months, there is an asymmetry in relation to the equator and this asymmetry presents a clear seasonal variation as already described in the previous section. *Forbes et al.* [2013] have discussed this topic simulating the dominance of migrating modes of the semidiurnal tide. They conclude that the latitudinal structure can be simulated by summing only few Hough modes [(2,2), (2,3), and (2,4)].

[28] *Pedatella and Forbes* [2010] observed that the lunar semidiurnal tide in the total electron content from November to February presented a significant hemispheric asymmetry. Numerical model by *Pedatella et al.* [2012b] showed that during January and July, the lunar semidiurnal tide amplitudes in the zonal and meridional neutral wind were hemispherically asymmetric, with the largest amplitudes occurring in the summer hemisphere. They also observed that the lunar semidiurnal tide in the zonal wind presented two period of significantly enhanced tidal amplitude, with maxima between December and January and from June to August. Furthermore, the maximum that occurred around December solstice was slightly larger.

[29] It is well known that the generation of the lunar tide has secondary contributions due to the vertical motion of the oceans. The great difference between the ocean area in the Northern and Southern Hemispheres will certainly affect in some way the lunar semidiurnal tide. However, only the global distribution of the oceans might not be sufficient to explain the seasonal variation of this asymmetry. Since the lunar tide is sensitive to the atmospheric conditions when it propagates upward, we believe that the wind system and temperature structures could contribute for this observed behavior.

[30] If the primary forcing of the lunar tide excites only migrating modes, the longitudinal variability would not appear. Figures 4, 5, and 6 present a clear longitudinal variability at three altitudes. The longitudinal structures are most pronounced at 90 and 108 km. *Pedatella and Forbes* [2010] also showed longitudinal variations in the lunar tides observed in the TEC measurements. *Pedatella et al.* [2012b] verified longitudinal variability in the lunar semidiurnal tide using numerical model, and they found that behavior was most evident at low latitudes.

[31] As observed in Figures 4 and 5, about four longitudinal peaks appear in the lunar tide amplitudes at some altitudes. One can see four peaks in (1) September, in Northern Hemisphere, mainly at 108 km; (2) December for both hemispheres at 108 km, but this structure is weaker in Northern Hemisphere; (3) at 90 km in Northern Hemisphere. These structures seem to be associated to a zonal wave 4 pattern. Wave 4 structures in the atmosphere have been largely observed using satellite data [*Sagawa et al.*, 2005; *Immel et al.*, 2006; *Zhang et al.*, 2006; *England et al.*, 2006; *Fejer et al.*, 2008]. *Forbes et al.* [2006] showed that the existence of DE3 is connected with the predominant wave 4 longitude distribution of topography and land-sea difference at low latitudes. *Zhang et al.* [2006] observed that the wave 4 patterns are due to interference between DW1, DE3, and DW5 for the diurnal tide and SW2, SE2, and SW6 for the semidiurnal tide.

[32] The theory of the lunar tide suggests that the migrating components are much larger than nonmigrating one. However, nonmigrating modes are capable of introducing longitudinal variations. So the nonmigrating components must be important for the global distribution of this tide. The existence of nonmigrating components might be due to ocean and solid Earth tidal forcing that propagate vertically or due to nonlinear interaction between stationary planetary waves and the migrating modes.

[33] In order to investigate the role of the nonmigrating components in the lunar semidiurnal tide, a two-dimensional least square fit, as done in *Pedatella et al.* [2012a], is performed to obtain both migrating and nonmigrating components. The fit is done by using the equation

$$\sum_{s=-6}^{7} A_s \cos(2\tau + (s-2)\lambda - \phi_s)$$

where, λ is longitude, τ is lunar local time (in radians), s denotes the zonal wave number, A_s and ϕ_s are the amplitude and phase of the lunar semidiurnal tide. The wave is propagating eastward for s negative and westward for s positive.

[34] Figure 7a shows the vector-averaged monthly mean amplitudes for lunar semidiurnal tide in December at 108 km. Figure 7b presents a reconstruction of amplitudes shown in Figure 7a based on the superposition of tidal components. Figure 7c exhibits the latitudinal variation of the amplitudes for both migrating (black line) and nonmigrating (colored lines) components used in the reconstruction shown in Figure 7b. The error bars represent the standard deviation, and the uncertainties in this climatology are due mainly to the well-known year-to-year variability of lunar tide as mentioned before. Here the notation SEs or SWs denote eastward or westward semidiurnal tide with zonal wave number s, respectively.

[35] In Figure 7a a clear longitudinal structure can be seen, which would not be observed if the lunar tide was composed only by the migrating component. The migrating semidiurnal component ($n = 2$, $s = 2$) is stronger than the nonmigrating ones at all latitudes, as expected. The amplitudes of the nonmigrating components are small (Figure 7c) and vary between 0 and 1.5 K, even though they are essential for the formation of the longitudinal structures.

[36] Small magnitudes showed in the climatological results are because the variability and a consequent self-cancelation associated with the vector average calculation. Although the migrating component is significantly larger, relatively small nonmigrating components are capable of introducing significant longitudinal structure, as shown by *Zhang et al.* [2006].

[37] Figure 7a can be well approximated by the sum of the dominant migrating component (SW2) with the following nonmigrating components: SE2 (red line + open circle), SE1 (light green line + cross), SW5 (blue line + filled pentagon), and SW6 (green line + diamond). The contribution of other nonmigrating tides is to add some details in the salient characteristics. Note that for either SE2 or SW6, $n = 2$, $|s - n| = 4$, which means that both of these components are connected to four longitudinal peaks. On the other hand, either SE1 or SW5 exhibit three peaks in longitude.

[38] *Zhang et al.* [2006] studied wave 4 pattern using SABER data and verified that the presence of this wave in solar semidiurnal tide is due to interference between SW2, SE2, and SW6. In the case of lunar semidiurnal tide, those components are very important in the reconstruction of longitudinal structures observed in December at 108 km. However, SW5 and SE1 are important as well.

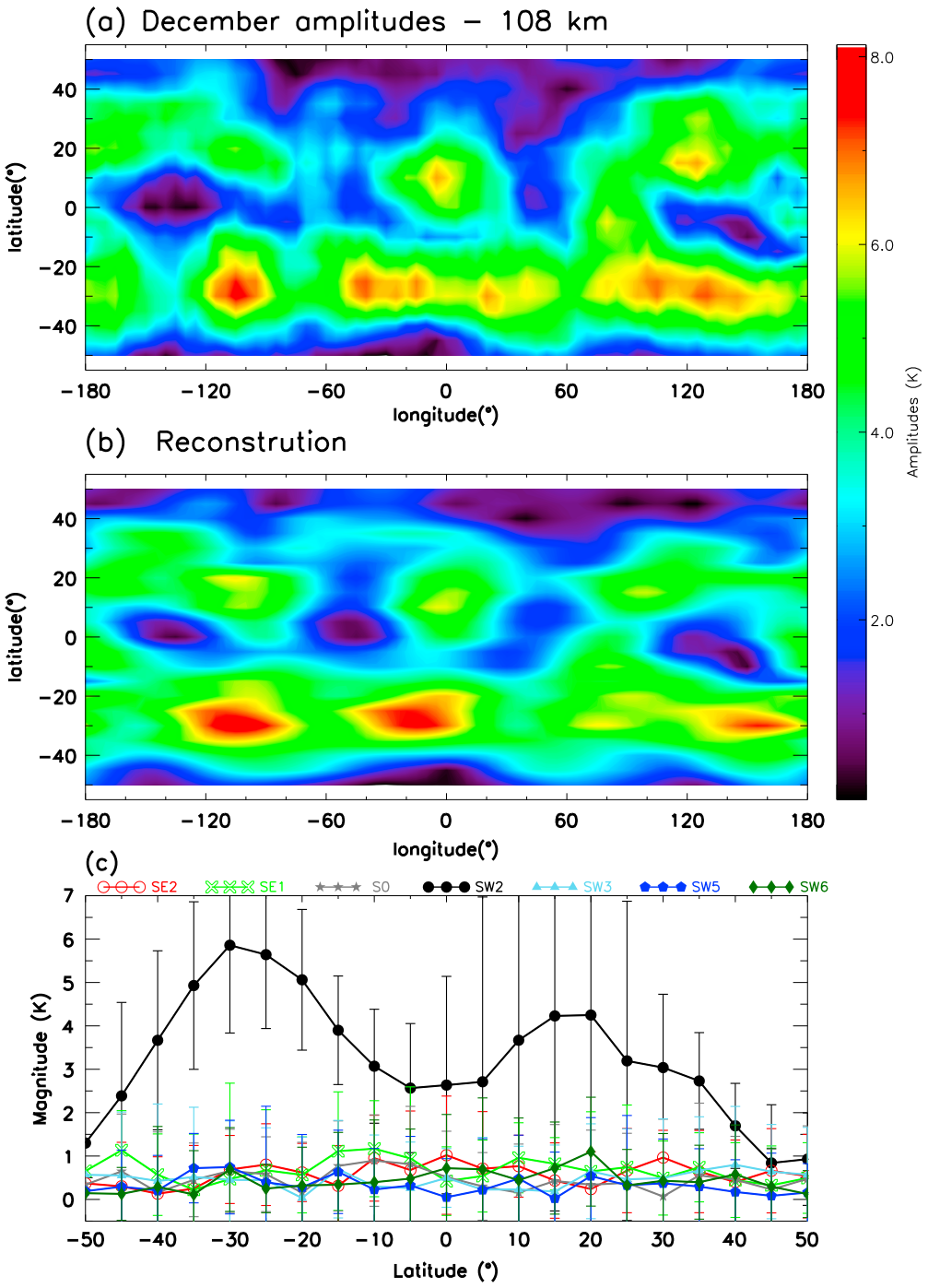

Figure 7. (a) Amplitude of the lunar semidiurnal tide for monthly mean December at 108 km altitude. (b) The reconstruction based on the superposition of tidal components. (c) Latitudinal distribution of the migrating (black line) and nonmigrating (colored lines) components.

[39] Figure 8 presents a similar analysis, but for a single year (2005), for the month of January at 108 km. As before, the error bars represent the standard deviation. Note that the error bars, in this case, are smaller than that presented in the climatological results. The main longitudinal structure shown in Figure 8a can be reproduced by combining only the dominant migrating tide SW2 (black line + filled circle) and the nonmigrating component SW4 (violet line + star). The other nonmigrating components are important to account for the details in the main structure. Here we verify the presence of wave 2 patterns due to SW4.

[40] The results shown in Figures 7 and 8 suggest that nonmigrating modes cannot be ignored in the study of the lunar semidiurnal tides as they are partly responsible for the longitudinal structure in the amplitudes of the lunar semidiurnal tide.

[41] Figure 9 exhibits the vertical profiles of the monthly mean amplitudes of the lunar semidiurnal tide for migrating and nonmigrating components in December from 70 to 115 km at 20°N and 20°S. For both latitudes (Figures 9a and 9b) in the altitude interval between 70 and 90 km,

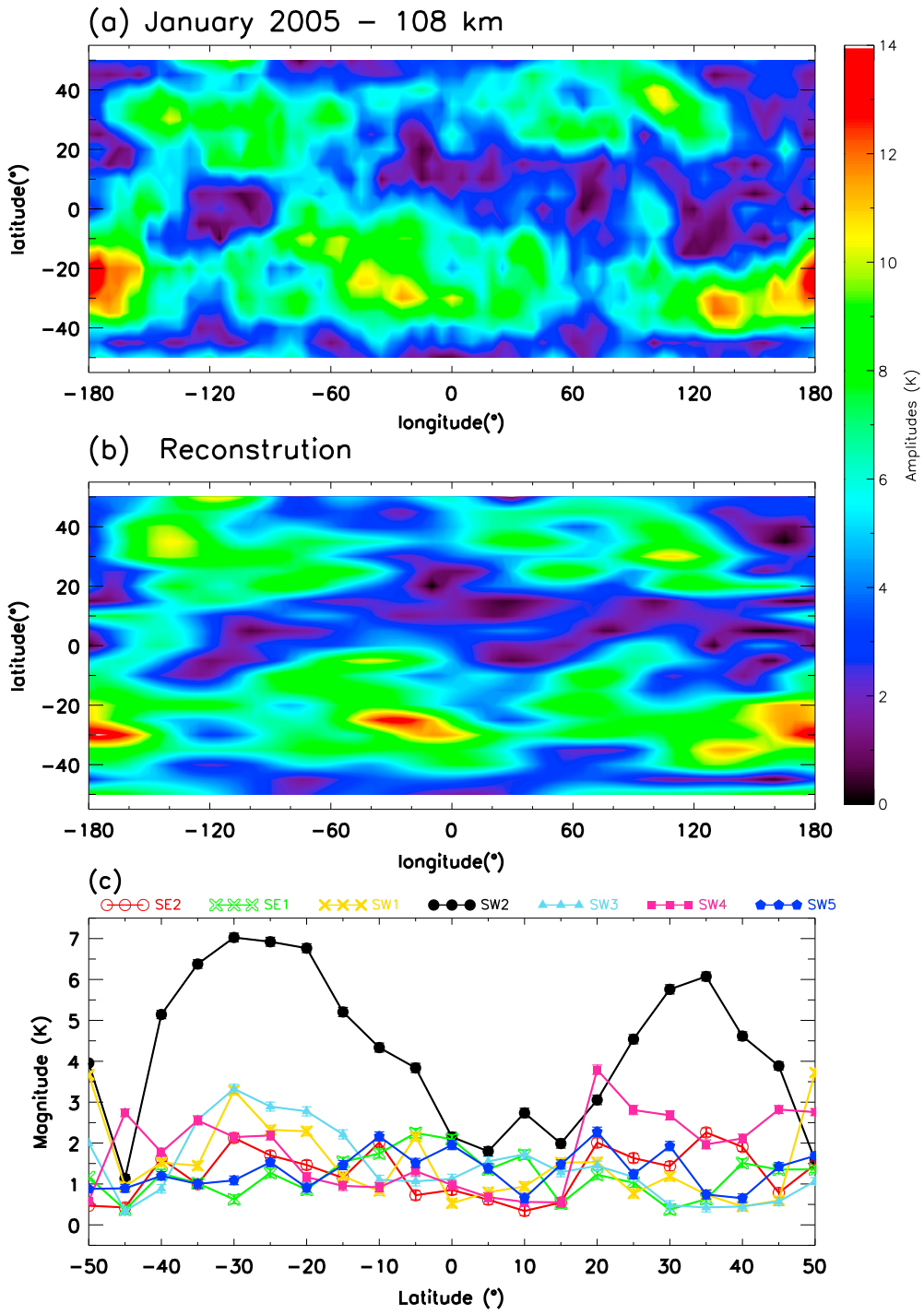

Figure 8. (a) Amplitude of the lunar semidiurnal tide for January 2005 at 108 km altitude. (b) The reconstruction based on the superposition of tidal components. (c) Latitudinal distribution of the migrating (black line) and nonmigrating (colored lines) components.

the amplitude of the migrating tide is only ~30% to 50% stronger than the nonmigrating components. However, at some altitudes of that interval, the migrating and nonmigrating components have the same magnitude. However, in higher altitudes the migrating component is dominant. Between 100 and 114 km at 20°N there is a competition between the nonmigrating components, for example, SW6 is stronger from 104 to 110, but at 102 km, SW3 and SE2 are stronger.

[42] Figure 10 shows the vertical profile of the monthly mean phase of the migrating and nonmigrating tidal components for lunar semidiurnal tide in December from 70 to 115 km at latitudes 20°N and 20°S. The migrating tide has characteristics of upward propagate wave for both latitudes. Lunar tidal components SE2 (70–90 km), SE1, S0 (80–100 km), SW3 (70–100 km), SW5 (90–100 km), SW6 (70–100 km) at 20°N and SE1 (70–85 km, 100–114 km), S0 (75–108 km), SW6 (90–115 km) at 20°S have the same feature.

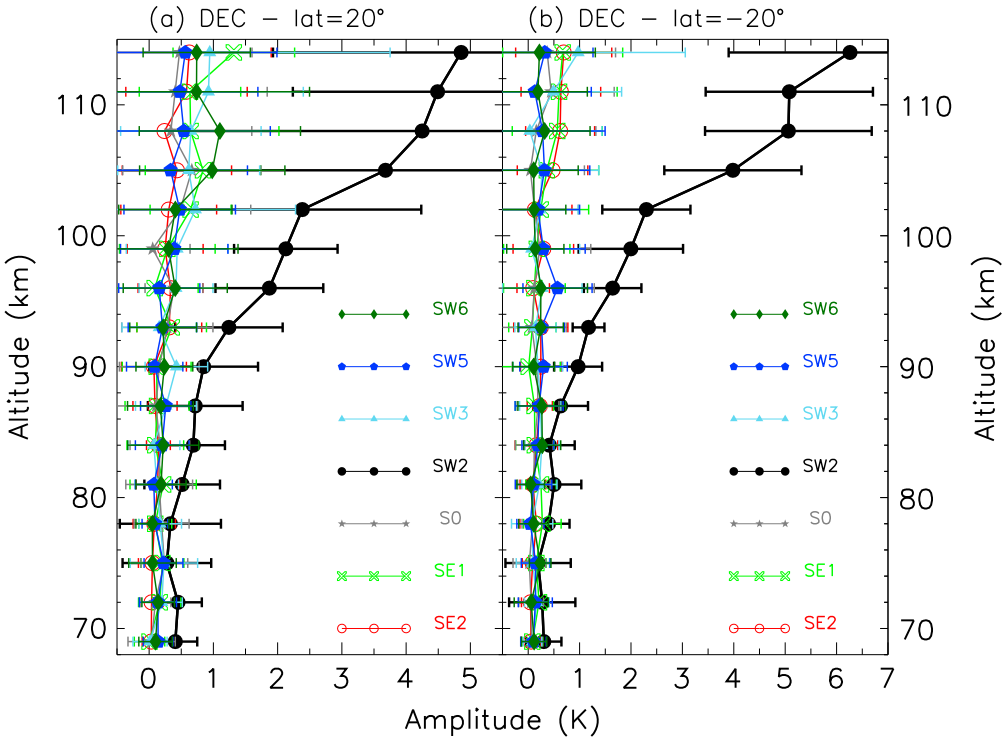

Figure 9. Vertical profiles of lunar semidiurnal tide amplitudes for migrating (black lines) and nonmigrating components (colored lines) at (a) 20° and (b) −20° latitude. These profiles were obtained for a representative December and were calculated using all available data for all December months.

[43] Figure 10 is useful to see how the longitudinal pattern can be drawn by considering constructive and destructive interference between different tidal components. For instance, at 108 km and at 20°N, the tidal components SE1 and SW5 are almost in phase producing wave 3 pattern. On the other hand, the components SW6 and SE2 are almost in antiphase reducing the magnitude of wave 4 pattern. This is in accordance with the results seen in Figure 7a; the wave 3 is more pronounced at this latitude.

[44] Figure 11 is similar to Figure 9 but for a single year (2005) for the month of January in 30°N (Figure 11a) and 30°S (Figure 11b). In this case, the competitions between the components at different altitudes are more pronounced. For 30°N latitude (Figure 11a) between 70 and 80 km the component SW1 is stronger than SW2. Besides, from 80 to 87 the component SW3 is stronger than SW2 and at 102 km the component SW3 becomes stronger again. From 104 to 110 the migrating component is dominant, but there is an alternation between the nonmigrating components.

[45] However, for 30°S (Figure 11b), from 70 to 80 the migrating and nonmigrating components present the same magnitude. From 80 to 90 km the migrating tide becomes stronger than the others, whereas, from 94 to 100 km the components SW4 and SW1 are stronger than migrating tide. Further, from 100 to 114 km the migrating component became dominant.

[46] *Haurwitz and Cowley* [1969] suggested that in the case of lunar tide oscillation, waves with wave numbers different from 2 may also be partly produced by mountain ranges, different frictional properties of continental and ocean surfaces, unequal distribution of temperature and wind systems which can modify the atmospheric response to the lunar tidal potential, and the tide of the ocean.

[47] The dominance of different tidal components at different altitudes may help to explain why the longitudinal structure of the lunar semidiurnal tide changes with the altitudes. To a better understanding of the importance of each component of the lunar semidiurnal tide, a more detailed study is required and it is out of the scope of the present paper.

[48] In order to explain the presence of wave 4 structure in the lunar tide and why that structure was verified in December and September, a detailed study is necessary. Furthermore, the presence of wave 4 structures in the amplitude fields of the lunar tide was pronounced for higher altitudes. For instance, below 80 km altitude, no similar behavior was observed. This suggests that the interaction between the lunar tide and other tides and/or other waves must be more expressive in the lower thermosphere region.

5. Summary

[49] The present study used the temperature measurements by SABER instrument in order to observe the dependence of the atmospheric lunar semidiurnal tide on latitude, longitude, and season, extending from ±50° latitude and 20–120 km altitude. The methodology is applied to over about 60 day intervals centered on each month.

[50] The vector average monthly amplitude over all period demonstrated that the lunar semidiurnal tide has characteristic of vertically propagating wave. The lunar semidiurnal tide propagates into the thermosphere and achieves maximum amplitudes in the height of ionospheric *E* region. In general, the maximum amplitudes are observed in the solstice months and the minimum in the equinox months.

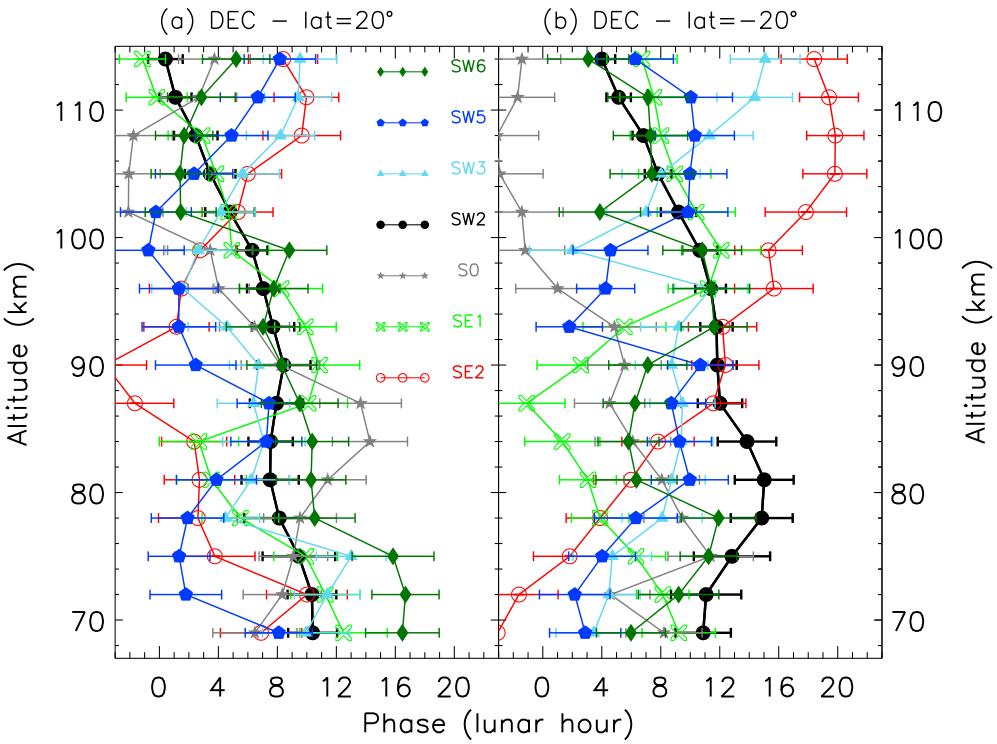

Figure 10. Vertical profiles of lunar semidiurnal tide phases for migrating (black lines) and nonmigrating components (colored lines) at (a) 20° and (b) −20° latitude. These profiles were obtained for a representative December and were calculated using all available data for all December months.

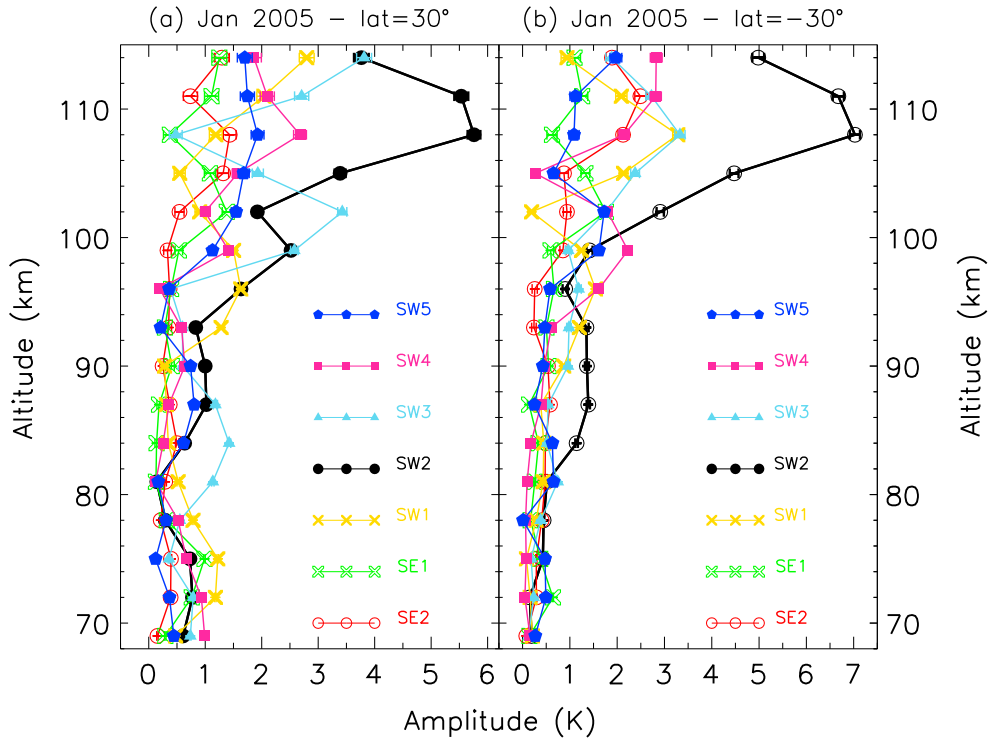

Figure 11. Vertical profiles of lunar semidiurnal tide amplitudes for migrating (black lines) and nonmigrating components (colored lines) at (a) 30° and (b) −30° latitude. These profiles are for a single year, January 2005 at 108 km.

[51] Lunar semidiurnal tide presented an asymmetric behavior in relation to the equator during the year and a significant longitudinal variability is also observed. These results suggest that asymmetric modes contribute significantly for this oscillation in the atmosphere and the interaction with other waves must be more pronounced, primarily in the high altitudes.

[52] Besides, the longitudinal variability reveals the existence of nonmigrating components in addition to the dominant migrating gravitational tide. The form of the longitudinal structures can be obtained by superposing the migrating and some dominant nonmigrating components. In December at 108 km, the horizontal pattern in the amplitudes of the lunar semidiurnal tide is due to SW2, SW6, SW5, SE2, and SE1.

[53] **Acknowledgments.** The authors are grateful to the SABER team for the access to the data on http://saber.gats-inc.com. This work has been supported by CNPq (Conselho Nacional de Desenvolvimento Científico e Tecnológico).

References

Bevington, P. R. (1969), *Data Reduction and Error Analysis for the Physical Sciences*, McGraw-Hill Book Company, New York.

Chapman, S., and R. S. Lindzen (1970), *Atmospheric Tides*, Gordon and Breach, Newark, N. J.

England, S. L., S. Maus, T. J. Immel, and S. B. Mende (2006), Longitudinal variation of the E-region electric fields caused by atmospheric tides, *Geophys. Res. Lett.*, *22*, L21105, doi:10.1029/2006GL027465.

Fejer, B. G., J. W. Jensen, and S.-Y. Su (2008), Quiet time equatorial F region vertical plasma drift model derived from ROCSAT-1 observations, *J. Geophys. Res.*, *113*, A05354, doi:10.1029/2007JA012801.

Fejer, B. G., M. E. Olson, J. L. Chau, C. Stolle, H. Lühr, L. P. Goncharenko, K. Yumoto, and T. Nagatsuma (2010), Lunar-dependent equatorial ionospheric electrodynamic effects during sudden stratospheric warmings, *J. Geophys. Res.*, *115*, A00G03, doi:10.1029/2010JA015273.

Forbes, J. M. (1982), Atmospheric tides 2. The solar and lunar semidiurnal components, *J. Geophys. Res.*, *87*, 5241–5252.

Forbes, J. M., and D. F. Gillete (1982), A compendium of theoretical atmospheric tidal structures, *AFGL Tech. Rep.*

Forbes, J. M., J. Russell, S. Miyahara, X. Zhang, S. Palo, M. Mlynczak, C. J. Mertens, and M. E. Hagan (2006), Troposphere-thermosphere tidal coupling as measured by the SABER instrument on TIMED during July-September 2002, *J. Geophys. Res.*, *111*, A10S06, doi:10.1029/2005JA011492.

Forbes, J. M., X. Zhang, S. Bruinsma, and J. Oberheide (2013), Lunar semidiurnal tide in the thermosphere under solar minimum conditions, *J. Geophys. Res. Space Phys.*, *118*, 1788–1801, doi:10.1029/2012JA017962.

García-Comas, M., et al. (2008), Errors in Sounding of the Atmosphere using Broadband Emission Radiometry (SABER) kinetic temperature caused by non-local-thermodynamic-equilibrium model parameters, *J. Geophys. Res.*, *113*, D24106, doi:10.1029/2008JD010105.

Haurwitz, B., and D. Cowley (1969), The lunar barometric tide, its global distribution and annual variation, *Pure Appl. Geophys.*, *77*, 122–150.

Immel, T. J., E. Sagawa, S. L. England, S. B. Henderson, M. A. Hagan, S. B. Mende, H. U. Frey, C. M. Swenson, and L. J. Paxton (2006), Control of equatorial ionospheric mosphology by atmospheric tides, *Geophys. Res. Lett.*, *33*, L15108, doi:10.1029/2006GL026161.

Lühr, H., T. A. Siddiqui, and S. Maus (2012), Global characteristics of the lunar tidal modulation of the equatorial electrojet derived from CHAMP observations, *Ann. Geophys.*, *30*, 527–536, doi:10.5194/angeo-30-527-2012.

Mertens, C. J., M. G. Mlynczak, M. López-Puertas, P. P. Wintersteiner, R. H. Picard, J. R. Winick, L. L. Gordley, and J. M. Russell III (2001), Retrieval of mesospheric and lower thermospheric kinetic temperature from measurements of CO2 15 μm Earth Limb Emission under non-LTE conditions, *Geophys. Res. Lett.*, *28*(7), 1391–1394.

Mertens, C. J., et al. (2009), Kinetic temperature and carbon dioxide from broadband infrared limb emission measurements taken from the TIMED/SABER instrument, *Adv. Space Res.*, *43*(1), 15–27.

Park, J., H. Luhr, M. Kunze, B. G. Fejer, and K. W. Min (2012), Effect of sudden stratospheric warming on lunar tidal modulation of the equatorial electrojet, *J. Geophys. Res.*, *117*, A03306, doi:10.1029/2011JA017351.

Paulino, A. R., P. P. Batista, B. R. Clemesha, R. A. Buriti, and N. Schuch (2012), An enhancement of the lunar tide in the MLT region observed in the Brazilian sector during 2006 SSW, *J. Atmos. Sol. Terr. Phys.*, *90–91*, 97–103, doi:10.1006/j.jastp.2011.12.015.

Pedatella, N. M., and J. M. Forbes (2010), Global structure of the lunar tide in ionospheric total electron content, *Geophys. Res. Lett.*, *37*, L06103, doi:10.1029/2010GL042781.

Pedatella, N. M., H. L. Liu, A. D. Richmond, A. Maute, and T.-W. Fang (2012a), Simulations of solar and lunar tidal variability in the mesosphere and lower thermosphere during sudden stratosphere warmings and their influence on the low-latitude ionosphere, *J. Geophys. Res.*, *117*, A08326, doi:10.1029/2012JAO17858.

Pedatella, N. M., H. L. Liu, A. D. Richmond, A. Maute, and T.-W. Fang (2012b), Atmospheric semidiurnal lunar tide climatology simulated by the Whole Atmosphere Community Climate Model, *J. Geophys. Res.*, *117*, A06327, doi:10.1029/2012JAO17792.

Ray, R. D., and S. B. Luthcke (2006), Tide model errors and Grace gravimetry: Towards a more realistic assessment, *Geophys. J. Int.*, *167*, 1055–1059, doi:10.1111/j.1365-246X.2006.03229.x.

Remsberg, E. E., et al. (2008), Assessment of the quality of the Version 1.07 temperature-versus-pressure profiles of the middle atmosphere from TIMED/SABER, *J. Geophys. Res.*, *113*, D17101, doi:10.1029/2008JD010013.

Sagawa, E., T. J. Immel, H. U. Frey, and S. B. Mende (2005), Longitudinal structure of the equatorial anomaly in the nighttime ionosphere observed by IMAGE/FUV, *J. Geophys. Res.*, *110*, A11302, doi:10.1029/2004JA010848.

Stening, R. J., and C. Jacobi (2001), Lunar tidal winds in the upper atmosphere over Collm, *Ann. Geophys.*, *18*, 1645–1650.

Stening, R. J., A. H. Manson, C. E. Meek, and R. A. Vincent (1994), Lunar tidal winds at Adelaide and Saskatoon at 80 to 100 km heights: 1985–1990, *J. Geophys. Res.*, *99*, 13,273–13,280.

Stening, R. J., J. M. Forbes, M. E. Hagan, and A. D. Richmond (1997), Experiments with a lunar atmospheric tidal model, *J. Geophys. Res.*, *102*, 13,465–13,471.

Vial, F., and J. M. Forbes (1994), Monthly simulations of the lunar semidiurnal tide, *J. Atmos. Terr. Phys.*, *56*, 1591–1607.

Zhang, X., J. M. Forbes, M. E. Hagan, J. M. Russell, S. E. Palo, C. J. Mertens, and M. G. Mlynczak (2006), Monthly tidal temperatures 20–120 km from TIMED/SABER, *J. Geophys. Res.*, *111*, A10S08, doi:10.1029/2005JA011504.